Nano Energy 107 (2023) 108145

Contents lists available at ScienceDirect

Nano Energy

journal homepage: www.elsevier.com/locate/nanoen

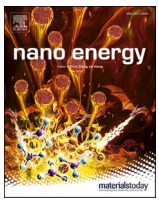

Engineering a wirelessly self-powered and electroconductive scaffold to promote peripheral nerve regeneration

Yafeng Yang [a,1], Xin Yin [a,1], Huadong Wang [a,1], Wenqi Qiu [b], Li Li [a], Fenglu Li [b], Yizhu Shan [c], Ziteng Zhao [a], Zhou Li [c,*], Jidong Guo [a,*], Jin Zhang [b,*], Yantao Zhao [a,d,**]

[a] Senior Department of Orthopedics, the Fourth Medical Center of PLA General Hospital, Beijing 100048, China
[b] Qingyuan Innovation Laboratory, 1 Xueyuan Road, Quanzhou 362801, P. R. China
[c] Beijing Institute of Nanoenergy and Nanosystems, Chinese Academy of Sciences, Beijing 101400, China
[d] Beijing Engineering Research Center of Orthopedics Implants, Beijing 100048, China

ARTICLE INFO

Keywords:
Composite scaffold
Soft hydrogel
Self-powered
Electroconductive
Peripheral nerve regeneration

ABSTRACT

Electroactive biomaterials have been shown useful for the repair of injured peripheral nerve. While for conventional conductive conduits, outer electrical stimulation device is unavoidably employed to exert electrical signals, and their rigid microstructures are usually incompatible with neural cells. Herein, a soft carbon nanotubes@gelatin methacryloyl/poly(L-lactic acid) (CNTs@GelMA/PLLA) nerve tissue-engineering scaffold was fabricated, which provided an endogenous piezoelectric stimulation and conductive microenvironment. Based on amounts of *in-vitro* experiment data, such composite scaffold significantly improved adhesion and elongation of Schwann cells, and meanwhile promoted axonal outgrowth and neurites number of dorsal root ganglions. More interestingly, the scaffold was applied to a 10-mm sciatic nerve defect in rats and harvested at 12 weeks post-implantation. Immunohistochemical staining results indicated that our proposed graft significantly facilitated peripheral nerve regeneration by promoting myelination and axon outgrowth, meanwhile an enhanced motor functional recovery caused by the scaffold was also revealed due to the obviously-improved sciatic functional index and muscle weights. Overall, the soft, self-powered, and electroconductive CNTs@GelMA/PLLA scaffold is a promising candidate for the treatment of peripheral nerve injuries.

1. Introduction

Peripheral nerve injury (PNI) usually results in dysfunctions of target tissue and therefore severely affects living qualities of patients [1,2]. Autologous nerve graft has been considered as “gold standard” for PNI repair, while lack of suitable donor nerves and high morbidity at surgical sites limit its clinic applications [3]. With the developments of tissue engineering and biomaterials, artificial nerve scaffolds are regarded as potential candidate for peripheral nerve regeneration. Especially for the electroactive scaffolds, the employment of which along with electrical stimulation have been demonstrated with abilities of regulating neural cell behaviors such as neural differentiation, maturation, secretion, axon outgrowth, and remyelination [4–9]. Nevertheless, traditional electroactive scaffolds have some drawbacks such as inflammation or infection caused by invasively-implanted electrodes, the second surgery to remove implants, as well as incompatibility between rigid structure of conduits and neural cells [10,11]. Therefore, it is of great necessity to design a kind of wireless, biocompatible, and soft electroactive scaffolds for the repair of PNI.

Piezoelectric materials belong to smart materials with capability of converting mechanical forces into electrical signals, thus piezoelectric scaffolds can be utilized as wireless electrical stimulators to promote tissue repair and regeneration [12,13]. It was reported that the exercise-induced piezoelectric poly(L-lactic acid) (PLLA) scaffold could promote cartilage regeneration in rabbits [14]. In addition, Guo *et al.* successfully fabricated a piezoelectric biomaterial by coating piezoelectric $BaTiO_3$ nanoparticles onto Ti6Al4V scaffold, and the *in-vitro* and *in-vivo* results showed that the piezoelectric effect could significantly promote osteogenesis and angiogenesis [15]. However, applications of some traditional piezoelectric materials such as polyvinylidene fluoride,

* Corresponding authors.
** Corresponding author at: Senior Department of Orthopedics, the Fourth Medical Center of PLA General Hospital, Beijing 100048, China.
E-mail addresses: zli@binn.cas.cn (Z. Li), gjd304@126.com (J. Guo), J_Zhang929@fzu.edu.cn (J. Zhang), biodoctor1981@163.com (Y. Zhao).
[1] These authors equally contributed to this work.

https://doi.org/10.1016/j.nanoen.2022.108145
Received 19 November 2022; Received in revised form 12 December 2022; Accepted 24 December 2022
Available online 26 December 2022

zinc oxide, and lead zirconate titanate in the nerve tissue-engineering field are generally limited, due to their non-biodegradability and toxicity [14]. PLLA as a well-known U.S. Food and Drug Administration-approved biomaterial, is also an ideal piezoelectric polymer with excellent biodegradable and biocompatible properties [16]. The electrospinning process is demonstrated to induce PLLA piezoelectricity by changing orientation of C═O dipoles of PLLA from random to orderly [12]. Liu *et al.* once reported that electricity generated by PLLA nanofibers significantly promoted expansion and proliferation of neural stem cells (NSCs) [17]. Furthermore, well-aligned structure of the nerve conduit obtained in our previous study was demonstrated with an ideal topographical guidance for the repair of PNI [8], which gave us lots of insights choosing aligned electrospinning PLLA nanofibers as a preferred material for preparing wireless self-powered nerve scaffold.

A soft and moist extracellular matrix (ECM) microenvironment is also very crucial for neural cells activities including adhesion, proliferation, differentiation, and secretion [18–20]. Hydrogels are promising biomaterials for mimicking ECM due to their high water content, excellent biocompatibility, and adjustable mechanical flexibility. Among them, gelatin methacrylate (GelMA) hydrogel contains many arginine-glycine-aspartic acid (RGD) sequences and low antigenicity, being widely employed as a platform to verify cell activities. For instance, a composite material including super-aligned carbon nanotubes (CNTs) sheet and GelMA hydrogel was proposed to promote growth of spiral ganglion neurons [21]. Meanwhile, an imidazole groups-functionalized GelMA hydrogel was developed to enhance neural differentiation of human amniotic mesenchymal stromal cells [22]. Regarding electrical exciting property of neuronal cells, electroconductive property of the neural conduits is also considerable important for nerve regeneration. Therefore, besides the construction of a wireless self-powered and rigid shell, a soft and biomimetic conductive microenvironment inside the scaffold is highly desired for realizing an efficient repair of PNI.

In the current study, electrospun piezoelectric PLLA nanofibers with well-aligned structure were first fabricated as shell materials of nerve conduits. At the meantime, as an ideal electroactive content with high electrical conductivity and low cytotoxicity, CNTs were homogeneously incorporated into GelMA solution to develop a soft and conductive hydrogel [23]. To afford a biomimetic microenvironment for neural cells, such conductive CNTs@GelMA composite hydrogel was embedded into the aligned electrospun PLLA piezoelectric conduit to acquire the resultant CNTs@GelMA/PLLA scaffold (Scheme 1). Such double-layer and electroconductive nerve tissue-engineering scaffold exhibited a suitable mechanical strength of ~ 10 kPa inside, matching stiffness requirement of the natural neural tissue perfectly [24]. More interestingly, mild electricity on the PLLA nanofibers surface generated by body movements was transferred to nerve fibers and Schwann cells through the conductive CNTs@GelMA hydrogel, so as to change cell membrane potential and increase cell excitability [25]. Based on amounts of *in-vitro* and *in-vivo* data, our proposed wirelessly self-powered and electroconductive CNTs@GelMA/PLLA scaffold with accelerated axonal growth, promoted remyelination regeneration, and improved nerve function recovery, would become a practical and efficient graft for comprehensively enhancing peripheral nerve regeneration.

2. Experimental section

2.1. Fabrication of CNTs@GelMA/PLLA scaffold

PLLA pellets were dissolved in 1,1,1,3,3,3-hexafluoroisopropanol (HFIP) solvent at a concentration of 15 % (*W/V*) to form an electrospinning solution. Then, the solution was drawn into a 10.0 mL-syringe and flowed at the rate of 0.3 mm/min by a syringe pump. A positive high voltage power supply connected to the syringe needle was set to be 16 kV and a negative voltage was also applied to be − 1 kV. Distance between the syringe needle and the collector was predetermined as 18.0 cm. The PLLA fibers were harvested on an aluminum foil that was covered on a rotating collector. To obtain PLLA films, rotation speeds of the collector were set as 100 rpm (non-aligned fibers) and 5000 rpm (aligned fibers). To make an aligned conduit, two stainless steel saw blades were placed in parallel 5.0 mm before the collector. Then, the two blades were applied with a negative high voltage power, which converted the disordered electrospunning PLLA fibers into aligned ones.

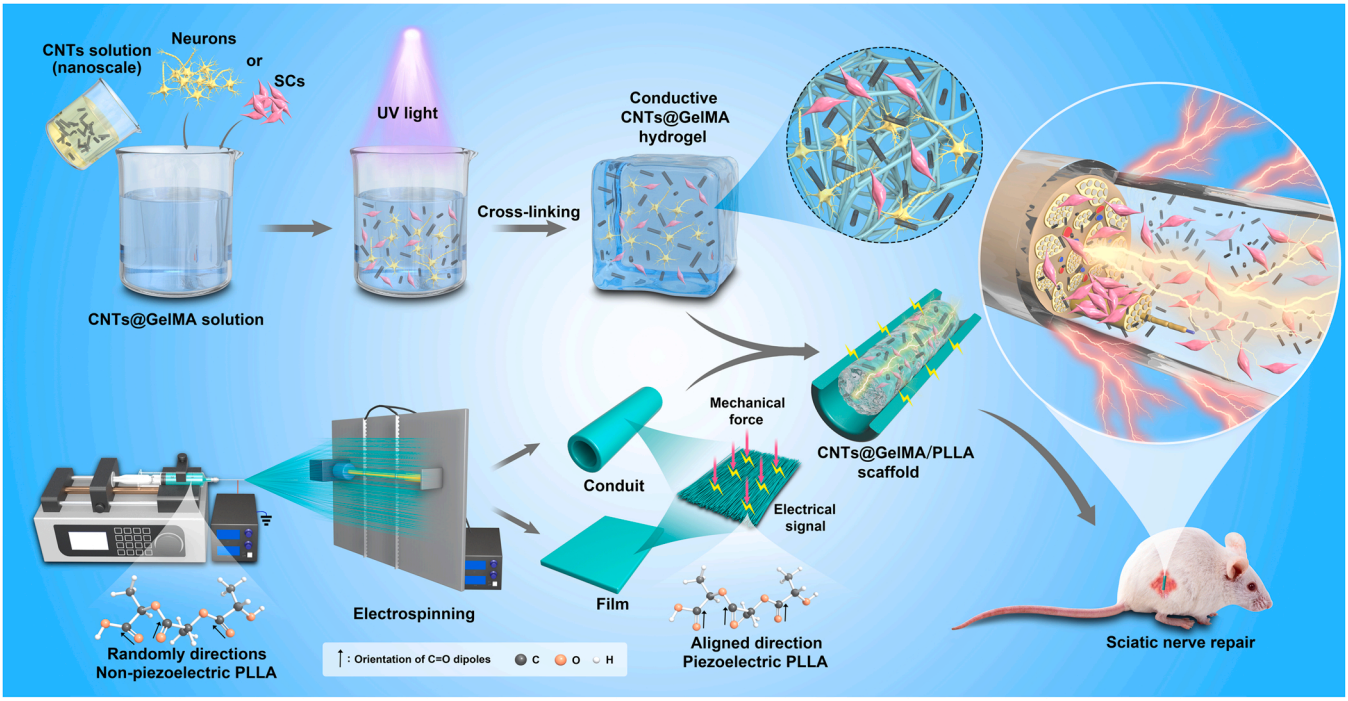

Scheme 1. Schematic illustration of manufacturing process and biomimetic application of wirelessly self-powered and electroconductive CNTs@GelMA/PLLA scaffold.

The resultant aligned PLLA conduit successfully simulated epineurium and provided a supporting effect for the inner encapsulated hydrogel.

Freeze-dried GelMA macromonomers were weighed and dissolved in distilled water at a concentration of 10% (*W/V*). Afterwards, the multiwalled CNTs (8–15 nm in diameter and ~ 50 μm in length) were added into the GelMA prepolymer solution at different concentrations of 0, 0.5, 1.0, and 2.0 mg/mL. The CNTs@GelMA solution was ultrasonicated for about 0.5 h in water bath and then the photoinitiator lithium phenyl-2,4,6-trimethylbenzoylphosphinate (LAP, 0.25%, *W/V*) was added (10%, *V/V*). To fabricate the CNTs@GelMA/PLLA composite film, the customized PLLA film was placed in 24-well plate, and then the CNTs@GelMA solution was added into the well and crosslinked under UV light exposure with an intensity of 30 mW/cm^2 for 30 s (15 s from the bottom layer and another 15 s from the top layer). To fabricate the CNTs@GelMA/PLLA composite scaffold, the homogeneous CNTs@GelMA and photoinitiator solution were drawn into a syringe and pre-crosslinked under UV light for 30 s. Then, the hydrogel was injected into the PLLA conduit.

2.2. Physical characterizations of CNTs@GelMA/PLLA scaffold

Topographic morphologies of the PLLA nanofibrous substrate and the CNTs@GelMA hydrogel were observed using a scanning electron microscopy (SEM, FEI Company, Hillsboro, OR, USA), where the hydrogels were gradually dehydrated, lyophilized, and then sputter-coated with a thin layer of gold at 25 °C. Porosities of these samples were analyzed by ImageJ software (Media Cybemetics, Rockville, MD, USA) based on the corresponding SEM images. The electrospinning PLLA film was dried at 60 °C for 24 h and cut into size of 1.5 × 1.5 cm^2, which were then analyzed by Fourier transform infrared spectroscopy (FTIR, Nicolet iS50, Waltham, MA, USA). X-Ray diffraction (XRD, Empyrean, PANalytical B.V, Almelo, Netherlands) was employed to characterize crystal structures of the samples. Testing patterns with Cu Kα radiation source were got at room temperature using a poly-functional X-ray diffractometer with a step size of 2°/min, and 2θ data between 5° and 70° were recorded.

Mechanical properties of the PLLA-based films including unaligned and aligned PLLA, GelMA/PLLA, and CNTs@GelMA/PLLA were examined following our previous protocols [8]. All the samples were cut into the standard rectangular strips with 5.0 × 1.0 cm^2 in size and approximately 0.3 mm in thickness before the examination. Stretching of the samples was performed in two opposite directions (0°) relative to the fiber orientation. All the examinations were performed at room temperature using a CMT-6104 Microcomputer-controlled electronic universal testing machine (Wanchen Test Machine Co. Ltd., Jinan, China) at a constant rate of 20.0 mm/min. From the stress–strain curves, Young's moduli and tensile strengths were accurately obtained. For the compression test, the hydrogel samples in each group were crosslinked under UV light and incubated in Phosphate Buffered Saline (PBS) at room temperature for 24 h. Then, they were conducted with an Instron 5524 mechanical analyzer (Instron, Canton, MA, USA). Both of the tensile and compressive mechanical performance were recorded and averaged for at least three specimens.

Conductivity of the CNTs@GelMA hydrogel was examined by the four-probe machine (RTS-8, Guangzhou Four-Point Probe Technology Co. Ltd., Guangzhou, China). Piezoelectric outputs of the aligned PLLA films were measured under an impact force of 20.0 N through a high impedance electrometer (Keithley 6517B, Cleveland, OH, USA). Piezoelectric force microscopy (PFM) was used for high resolution characterization and morphology imaging of piezoelectric responsive materials at 10 V in nanometer scale. Briefly, PLLA nanofibers were positioned on mica sheets using atomic force microscopy (AFM, Nanoscope V, Bruker, Dimension Icon, GER) in contact mode. Then, in PFM mode, three separate points were selected along the length direction of each fiber for single point spectral measurement. The AFM probe (AC240TM, Olympus, Tokyo, Japan) was aligned with the grounded silicon substrate and recorded its amplitude variation. In addition, the CNTs@GelMA hydrogel was immersed in PBS solution at 37 °C for 24 h to measure its swelling weight (W_s), which was then lyophilized to measure its dry weight (W_d). Swelling ratio of the CNTs@GelMA hydrogel was calculated according to the following Eq. (1):

$$Swelling\ ratio\ (\%) = \frac{W_s - W_d}{W_d} \times 100\% \quad (1)$$

2.3. In-vitro studies of CNTs@GelMA/PLLA scaffold

All the experimental procedures were conducted under direction of the Guide for the Care and Use of Laboratory Animals (National Institutes of Health Publication no. 85-23, revised 1985) and all the experiments were approved by the Ethics Committee of the Chinese People's Liberation Army General Hospital (Beijing, China). Dorsal root ganglion (DRG) neurons were harvested from neonatal Sprague Dawley rats (0–1 day) following an established method. Then, the DRGs were cultured on the CNTs@GelMA/PLLA composite scaffold and incubated in Neurobasal medium with 2.0% B-27% and 1.0% penicillin/streptomycin. The medium was replaced every 3 days. To generate localized electrical signals, the plates were placed in an ultrasonic homogenizer and the ultrasonic parameters were set to be 300 W for 10 min *per* day.

As previously described, the SCs were isolated from sciatic nerves of 1–2 days SD rats. Specifically, the sciatic nerves were harvested and the epineurium was removed under microscope. Then, the nerves were dissected and dissociated with 0.2% of type II collagenase and 0.25% trypsin at 37 °C for 20 min. Cells were seeded on the CNTs@GelMA/PLLA composite scaffold and maintained in Dulbecco's modified eagle medium containing 15.0% fatal bovine serum (FBS), 1.0% penicillin/streptomycin, 2.0 mM forskolin (Sigma-Aldrich, St. Louis, MO, USA), and 20.0 mg/mL bovine pituitary extract (Biomedical Technologies Inc., Stoughton, MA, USA) at 37 °C under humidified 5.0% CO_2. Passages 3–5 were used for the following experiments. To generate localized electrical signals, the plates were placed in an ultrasonic homogenizer and the ultrasonic parameters were set to be 300 W for 10 min *per* day.

LIVE/DEAD assays were performed in a 24-well plate according to the instructions. Briefly, 1.0 × 10^5/mL SCs were cultured on different concentrations of the CNTs@GelMA/PLLA composite scaffold (0, 0.5, 1.0, and 2.0 mg/mL) and incubated at 37 °C under humidified 5.0% CO_2 for 3 and 7 days. The cells were subjected to ultrasonic vibration for 10 min *per* day. Then, the samples were washed by PBS thrice and double-stained with calcein acetoxy methylester/propidium iodide double stain kit for 15 min at room temperature. The stained samples were finally observed under a confocal microscopy (TCS SP8, Leica, Wetzlar, Hesse, Germany).

The DRG, SCs, or sciatic nerves were washed with PBS thrice and fixed in 4.0% paraformaldehyde (PFA) for 20 min at room temperature. After being rinsed with PBS, the samples were permeabilized with 0.2% Triton-X for 30 min and blocked with 10.0% normal goat serum for 1 h. Then, the samples were incubated with primary antibodies at 4 °C overnight, including rabbit anti-rat β-3-tubulin (Tuj1, 1:200, ab52623, Abcam, UK), Neurofilament 160 (NF160, 1:200, ab254348, Abcam, UK), mouse anti-rat S100 (1:100, sc-53438, SANTA CRUZ, USA), and myelin basic protein (MBP, 1:200, ab11159, Abcam, UK). Subsequently, the samples were washed and incubated with goat anti-rabbit IgG H&L (CoraLite®488, 1:100, SA00013-2, Proteintech Group, Wuhan, China) or goat anti-mouse IgG H&L (CoraLite®594, 1:100, SA00013–3, Proteintech Group, Wuhan, China) secondary antibodies for 1 h at 37 °C. At last, cell nuclei of each group were stained with 4′,6-diamidino-2-phenylindole solution (DAPI, 1:500, ab228549, Abcam, UK) for 5 min at room temperature. The samples were ultimately observed and photographed with a confocal microscopy (TCS SP8, Leica, Wetzlar, Hesse, Germany), meanwhile neurite length and fluorescence intensity were measured with Image J software (Media Cybemetics, USA). To characterize dendrites of the neurons in different groups, sholl analysis was

implemented. In details, the images were first converted to grayscale images, and then the neurites were marked by Simple Neurite Tracer plugin in Image J software (Media Cybemetics, USA). The start radius was set to be 30.0 μm and the outer radius was determined as the longest neurite. Distance for each consecutive radius was set as 10.0 μm, and total/average numbers of crossing neurites for the DRG explants were calculated for analysis.

2.4. In-vivo studies of CNTs@GelMA/PLLA scaffold

All the animal experiments were conducted in accordance with the Guide for the Care and Use of Laboratory Animals (National Institutes of Health Publication no. 80-23, revised 1996) and approved by the Animal Care and Use Committee of Chinese PLA General Hospital (Beijing, China). Adult SD male rats weighing 220.0–240.0 g were intraperitoneally anaesthetized with 2.0% sodium pentobarbital solution (30.0 mg/kg animal weight). A skin incision around left thigh region was open and the sciatic nerve was exposed in a sterile environment, then an about 10.0-mm nerve segment was removed. In the autograft group, the 10.0-mm nerve segment was reversed 180° and sutured with 9/0 nylon sutures. For all the other groups, the nerve stumps in both sides were inserted 1.0-mm into a 12.0-mm PLLA or GelMA/PLLA or CNTs@GelMA/PLLA scaffold. Then, proximal and distal epineurium of the nerve stumps were sutured to the conduits. After closing the incision, the rats were intramuscularly injected with 80,000 units of penicillin and kept in warm and well-fed conditions.

To assess recovery of the motor function, the footprints were recorded by CATWalk XT system and Sciatic Function Index (SFI) was calculated at 6 and 12 weeks post-surgery according to the following Eq. (2):

$$\mathrm{SFI} = \frac{-38.3 \times (E\mathrm{PL} - N\mathrm{PL})}{N\mathrm{PL}} + \frac{109.5 \times (E\mathrm{TS} - N\mathrm{TS})}{N\mathrm{TS}} + \frac{13.3 \times (E\mathrm{IT} - N\mathrm{IT})}{N\mathrm{IT}} - 8.8 \quad (2)$$

N: non-operated foot; *E*: experimental foot; Print length (PL): distance from hindfoot to top of the 3rd toe; Intermediary toe spread (IT): distance between the 2nd and 4th toe; Toe spread (TS): distance between the 1st and 5th toe.

Electrophysiological assessments were conducted using an established method [8]. Briefly, the rats were anesthetized and sciatic nerves were exposed at 12 weeks. Electric impulse (3.0 mA, 1.0 Hz) was applied between proximal and distal nerve stumps, meanwhile amplitude and latency of the compound muscle action potentials (CMAPs) were recorded by inserting an electrode into the gastrocnemius muscle. The electrophysiological assessment assay was conducted using a PowerLab 4SP distal data acquisition system (Keypoint 3.02, Dantec Dynamics A/S, Copenhagen, Denmark).

To analyze regeneration of the myelin sheath in damaged area, the nerve samples were fixed in 2.0% glutaraldehyde, postfixed with 1.0% osmium tetroxide, and then embedded in epoxy resin. The ultrathin sections were stained with uranyl acetate and lead citrate and observed using a transmission electron microscope (TEM, Hitachi H-600, Tokyo, Japan). Finally, the myelin sheath thickness and mean diameter of the myelinated axons were measured by Image J software (Media Cybemetics, USA) from the acquired TEM images.

Gastrocnemius muscles (GM) in experimental side (GM(E)) and normal side (GM(N)) were harvested and weighed at 12 weeks after surgery. The muscle weight percentage was calculated according to the following Eq. (3). Lastly, mid-belly of the GM was fixed, stained with Masson trichrome, and observed under a microscope (TECNAI G2 F20, FEI Co., Hillsboro, OR, USA). At least five random fields *per* section were selected and analyzed with Image J software.

$$\text{GM weight } (\%) = \frac{GM(\mathrm{E})}{GM(\mathrm{N})} \times 100\% \quad (3)$$

2.5. Statistical analysis

All data are presented as mean ± standard deviation (SD). The results were statistically analyzed by GraphPad Prism software (version 8.0, San Diego, USA) according to one-way analysis of variance. Values of $^{*}P < 0.05$, $^{**}P < 0.01$, $^{\&}P < 0.05$, $^{\&\&}P < 0.01$, $^{\#}P < 0.05$, $^{\#\#}P < 0.01$, $^{\$}P < 0.05$ or $^{\$\$}P < 0.01$ were considered statistically significant.

3. Results and discussions

3.1. Physical characterizations of aligned electrospun PLLA conduit, CNTs@GelMA hydrogel, and composite CNTs@GelMA/PLLA scaffold

In our previous study, the fabricated PCL/CNTs composite conduit with aligned structure has been demonstrated with a positive promotion effect on the repair of PNI [8]. While, it was a pity that the contact between regenerated nerve fibers and conductive conduits was not very compact enough, and thus resulted in a compromise of electroconductive efficacy [26,27]. Similarly, applications of some conventional nerve tissue-engineering conduits are also severely limited due to incompatibility between rigid structure and neural tissue [28]. Herein, a biomimetic CNTs@GelMA/PLLA composite scaffold was fabricated by encapsulating the conductive CNTs@GelMA hydrogel into the aligned electrospun PLLA conduit. As shown in Fig. 1A, B, an axially oriented nanofibrous structure was presented in SEM image of the electrospun PLLA film, with a mean deviation angle and fiber diameter of about 5.32° ± 3.73° and 250.38 ± 46.31 nm, respectively. The FTIR results verified that structural characteristics of the PLLA were not changed through the electrospinning process (Fig. 1D). Piezoelectric property of the electrospun PLLA nanofibers was examined by PFM. The nanofibers showed a clear piezoelectric activity and surface potential of the film was about 7.3 mV (Fig. 1C). Furthermore, well-known butterfly-shaped curves were displayed in the PFM amplitude and phase graphs, which was a signature character for piezoelectric materials (Fig. 1E).

To further mimic the natural neural microenvironment, a series of soft CNTs@GelMA hydrogels with different CNTs concentrations were developed and their porous morphologies were displayed in Fig. 1F. In addition, the CNTs with high electrical conductivity and low cytotoxicity were homogeneously distributed on the GelMA hydrogel surface as revealed from high magnification SEM images, which laid a theoretical foundation for promoting nerve tissue regeneration through changing membrane potential of neural cells, increasing cell excitability, and bridging nerve defects [23]. As shown in Fig. 1G, the CNTs@GelMA hydrogels with different CNTs concentrations of 0.0, 0.5, 1.0, and 2.0 mg/mL were cross-linked and exhibited excellent shaping ability. In addition, the composite hydrogel could be easily injected without formation of any clogs.

As shown in Fig. 1H, I, porosities in the 0 CNTs-, 0.5 CNTs-, 1.0 CNTs-, and 2.0 CNTs-groups were 62.49% ± 4.28%, 58.03% ± 3.95%, 55.73% ± 7.08%, and 49.77% ± 4.34%, respectively. Similarly, there was no significant differences among all the groups with regard to the swelling ratio ($P > 0.05$), indicating that incorporation of little CNTs towards the hydrogel did not cause obvious changes of scaffold structure and hydrophilicity. Mechanical properties of the hydrogels were also carefully examined (Fig. 1J). It should be noted that all the four groups showed similar stiffness ranged from 9.94 ± 3.34 kPa to 12.93 ± 3.01 kPa, such appropriate Young's modulus well matched the mechanical properties requirements of the nerve cells growth microenvironment. Electroconductivity is another critical parameter for peripheral nerve regeneration. As displayed in Fig. 1K, conductivities of the 1.0 CNTs- and 2.0 CNTs-hydrogels were significantly higher than those in the 0 CNTs- and 0.5 CNTs-groups ($^{**}P < 0.01$). Consequently, such obtained CNTs@GelMA hydrogel showed good conductivity and similar stiffness to nerve tissue, which provided a beneficial

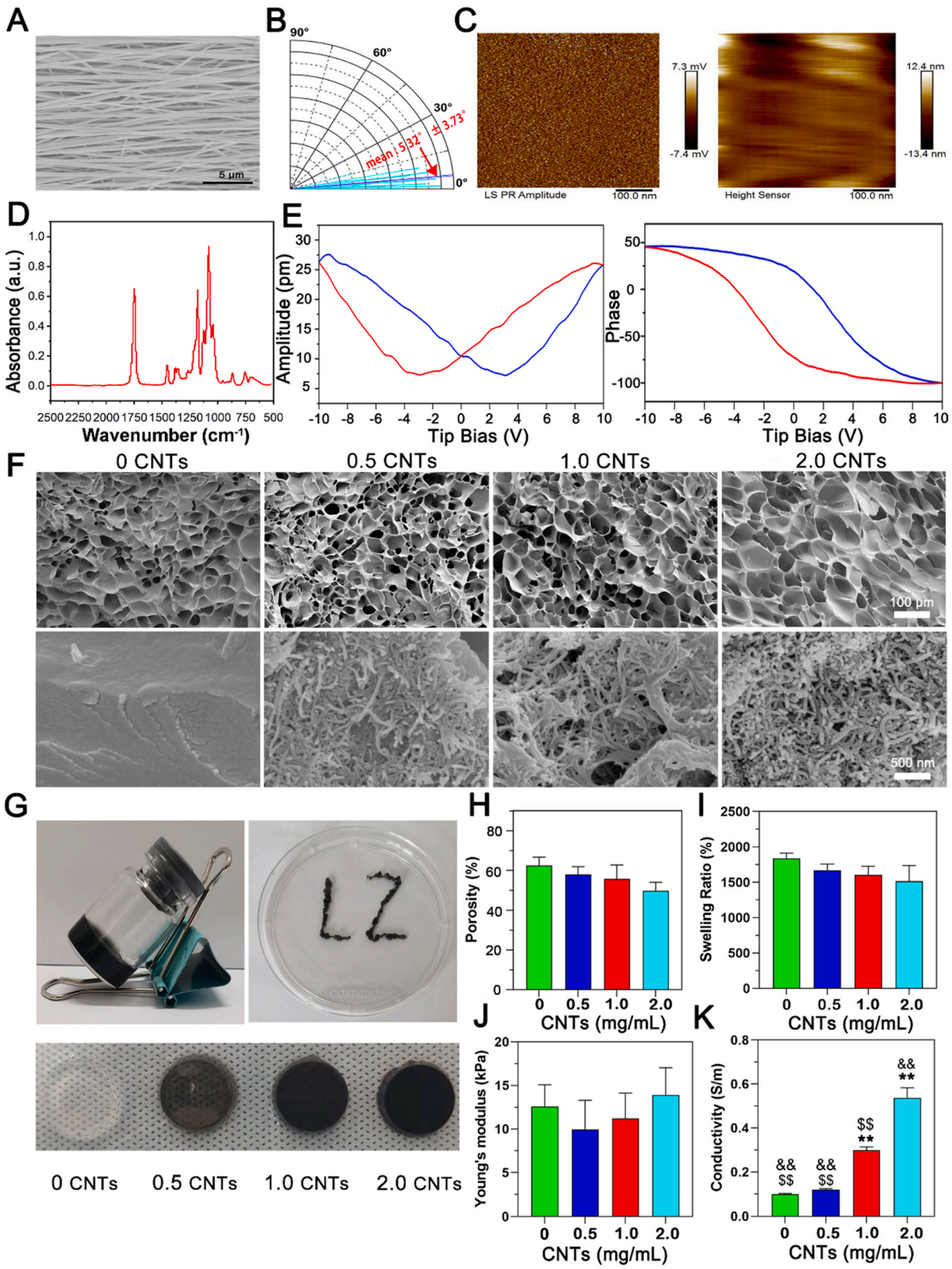

Fig. 1. Physical characterizations of electrospun PLLA nanofibers and CNTs@GelMA hydrogel. (A) SEM image, (B) mean deviation angle, (C) PFM graphs, (D) FTIR result, and (E) PFM amplitude and phase graphs of aligned electrospun PLLA nanofibers. (F) Representative SEM micrographs, (G) gross photographs, (H) porosity distributions, (I) equilibrium swelling ratios, (J) Young's moduli, and (K) electrical conductivities of CNTs@GelMA hydrogel with different concentrations of CNTs (0, 0.5, 1.0, and 2.0 mg/mL). All statistical data are represented as mean ± SD ($n = 3$; $^{**}P < 0.01$ for comparison with the 0 CNTs-group. $^{\&\&}P < 0.01$ for comparison with the 1.0 CNTs-group. $^{\$\$}P < 0.01$ for comparison with the 2.0 CNTs-group).

microenvironment for the repair and function recovery of PNI [29].

The CNTs@GelMA/PLLA composite scaffold was fabricated and observed by camera and SEM (Fig. 2A). Length of the scaffold was predetermined as about 12.0 mm, with an inner and outer diameter of 2.0 and 2.5 mm, respectively. Compared with the simple PLLA conduit, the CNTs@GelMA/PLLA scaffold showed a double-layer hierarchical structure, where honeycomb-like porous framework inside the hollow conduit well simulated extracellular matrix characteristics of native nerve tissue. As shown in Fig. 2B, the diffraction patterns of CNTs@GelMA/PLLA scaffold present three main diffraction peaks. A sharp and strong diffraction peak at $2\theta = 16.8^{\circ}$ due to the (200)/(110) reflection of the α-form orthorhombic crystal lattice of PLLA. In addition, the phases (100) and (004) were from the CNTs, and they were both slightly shifted [30,31].

Mechanical properties of the non-aligned and aligned PLLA-based films including PLLA, GelMA/PLLA, and CNTs@GelMA/PLLA were measured using a CMT-6104 testing machine. Yield stresses and elastic moduli in the aligned PLLA-based groups were significantly higher than those of the non-aligned groups (Fig. 2C–E), which was mainly attributed to the lower number of fibers along the non-aligned group [32]. However, no matter in the aligned or non-aligned groups, mechanical properties of the PLLA, GelMA/PLLA, and CNTs@GelMA/PLLA films

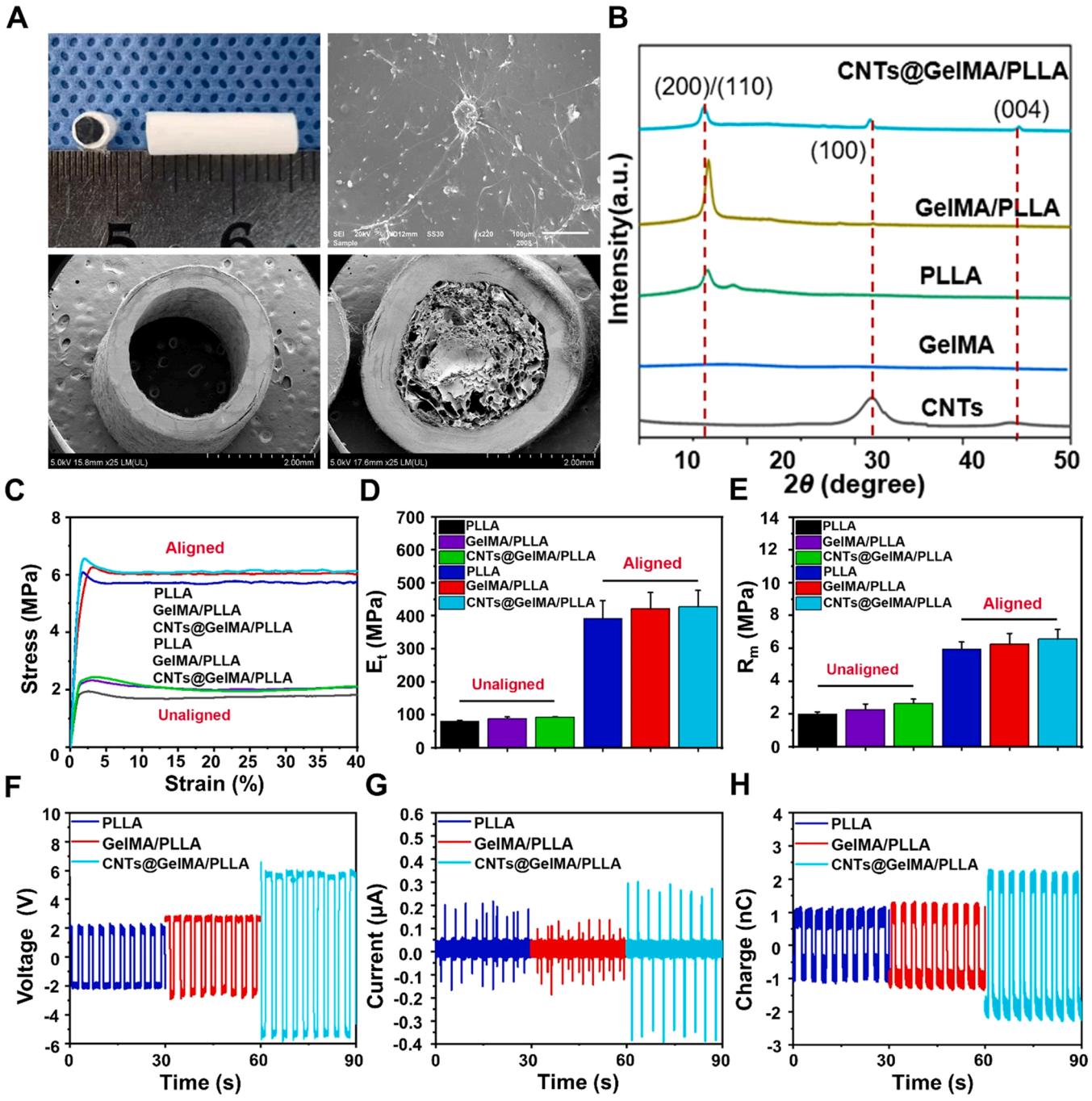

Fig. 2. Physical characterizations of composite CNTs@GelMA/PLLA scaffold. (A) Digital and SEM images of PLLA conduit and CNTs@GelMA/PLLA scaffold. (B) XRD curves of CNTs, GelMA, PLLA, GelMA/PLLA, and CNTs@GelMA/PLLA samples. (C) Tensile stress–strain curves, (D) Yield stresses and (E) elastic moduli of aligned and unaligned PLLA, GelMA/PLLA, and CNTs@GelMA/PLLA scaffolds. (F) Output voltage, (G) short-circuit current, and (H) output charge of aligned PLLA, GelMA/PLLA, and CNTs@GelMA/PLLA scaffolds.

showed no significant differences. Based on such optimal mechanical properties, the aligned PLLA-based scaffolds were employed for the following experiments.

Output charges, currents, and voltages of the aligned PLLA, GelMA/PLLA, and CNTs@GelMA/PLLA scaffolds were measured using an electrometer (Fig. 2F–H). Output voltages of the aligned PLLA and GelMA/PLLA were similar, which were 2.22 V and 2.86 V, respectively, but much lower than that in the aligned CNTs@GelMA/PLLA group (5.96 V). Similar tendency was found in terms of the charge and current results, which was because CNTs with good electrical conductivity formed a conductive network inside the hydrogel. And relatively-high conductivity allowed more electrons to be transferred to the external circuit, which further produced better power output [33].

3.2. *In vitro survival, growth, and spreading of SCs on CNTs@GelMA/PLLA scaffold*

SCs belong to important glia cells which are responsible for promoting nerve outgrowth and elongation [34]. To assess survival of the SCs on various CNTs@GelMA/PLLA scaffolds under ultrasonic

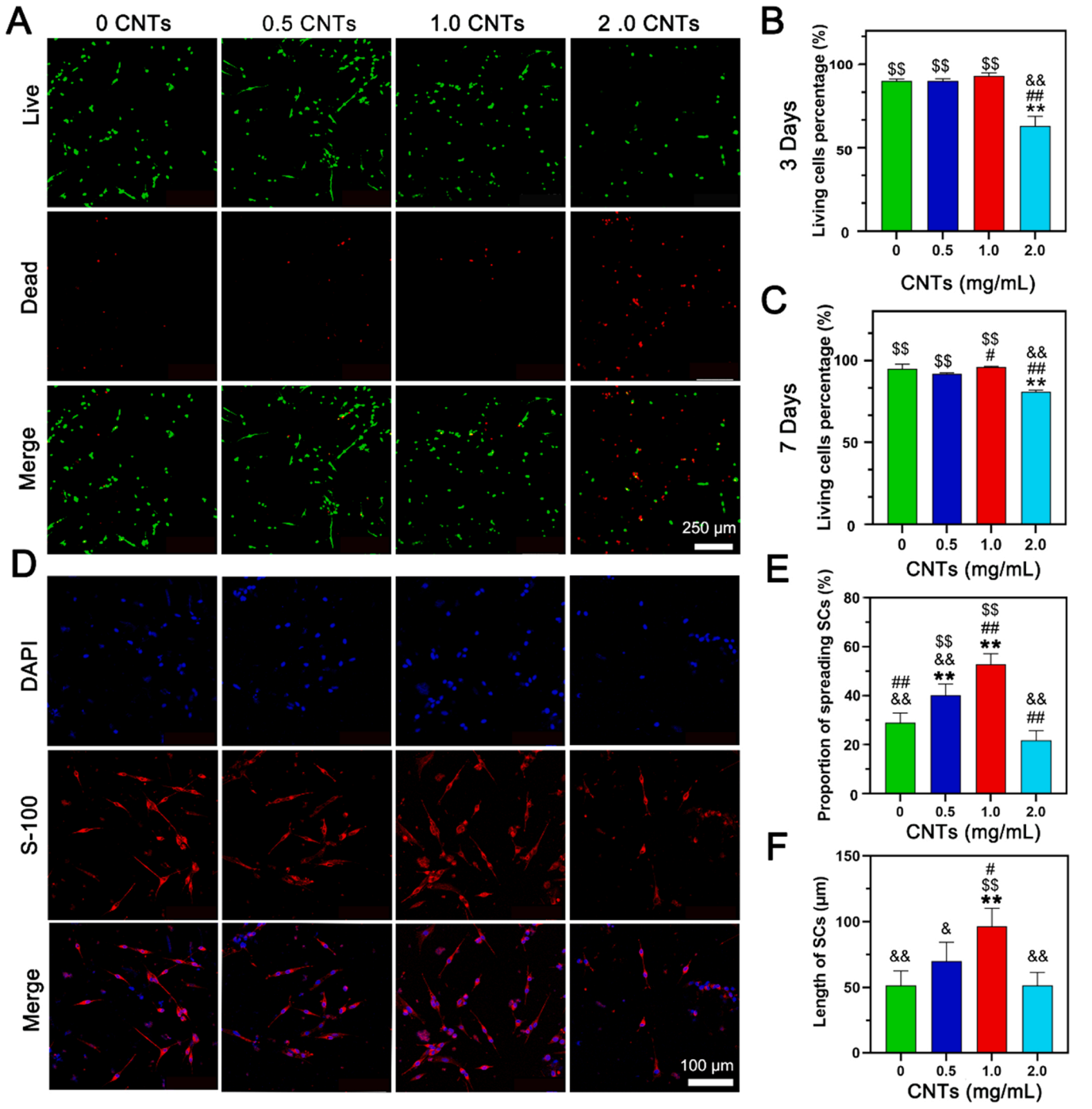

Fig. 3. *In-vitro* biocompatibility and cytotoxicity of CNTs@GelMA/PLLA scaffold. (A) LIVE/DEAD staining images. (B, C) Percentages of living cells at day 3 and 7. (D) S-100 fluorescence staining at day 7. (E) Spreading proportion and (F) average length of SCs cultured on various scaffolds. All statistical data are represented as mean ± SD ($n = 3$; ** $P < 0.01$ for comparison with 0 CNTs-group. $^{\#}P < 0.05$ for comparison with 0.5 CNTs-group. $^{\#\#}P < 0.01$ for comparison with 0.5 CNTs-group. $^{\&\&}P < 0.01$ for comparison with 1.0 CNTs-group. $^{\$\$}P < 0.01$ for comparison with the 2.0-CNTs group).

vibration, the LIVE/DEAD staining assay was performed at day 3 and 7. The number of living cells was similar among the 0 CNTs-, 0.5 CNTs-, and 1.0 CNTs-groups, but was significantly higher than that in the 2.0 CNTs-group (**$P < 0.01$, Fig. 3A–C).

Growth and spreading state of SCs were also evaluated by immunostaining assay. After 7 days under ultrasonic vibration, SCs in each group were immunostained with S-100 and observed under confocal microscope. Close to myelinated SCs, the morphology of SCs *co*-cultured with our fabricated CNTs@GelMA/PLLA scaffold was changed from spherical to bipolar along with time [35]. As shown in Fig. 3D, E, the percentage of bipolar and elongated SCs in the 1.0 CNTs-group was 53.00% ± 4.00% in the current study, which was higher than that in the 0 CNTs- (29.00% ± 4.00%, **$P < 0.01$), 0.5 CNTs- (40.00% ± 5.00%, **$P < 0.01$), and 2.0 CNTs-groups (22.00% ± 4.00%, **$P < 0.01$). Besides, length of the elongated SCs was 51.52 ± 10.98 μm, 69.99 ± 14.50 μm, 96.55 ± 13.61 μm, and 51.62 ± 9.77 μm in the 0 CNTs-, 0.5 CNTs-, 1.0 CNTs-, and 2.0 CNTs-groups, separately (Fig. 3F). All these results demonstrated that the CNTs@GelMA/PLLA scaffold with 1.0 mg/mL CNTs promoted the survival, adhesion, spreading, and myelination of SCs, providing an ideal platform for peripheral nerve regeneration.

3.3. *In-vitro* neurites outgrowth of DRGs on CNTs@GelMA/PLLA scaffold

DRGs as model of primary neurons have been widely-studied in

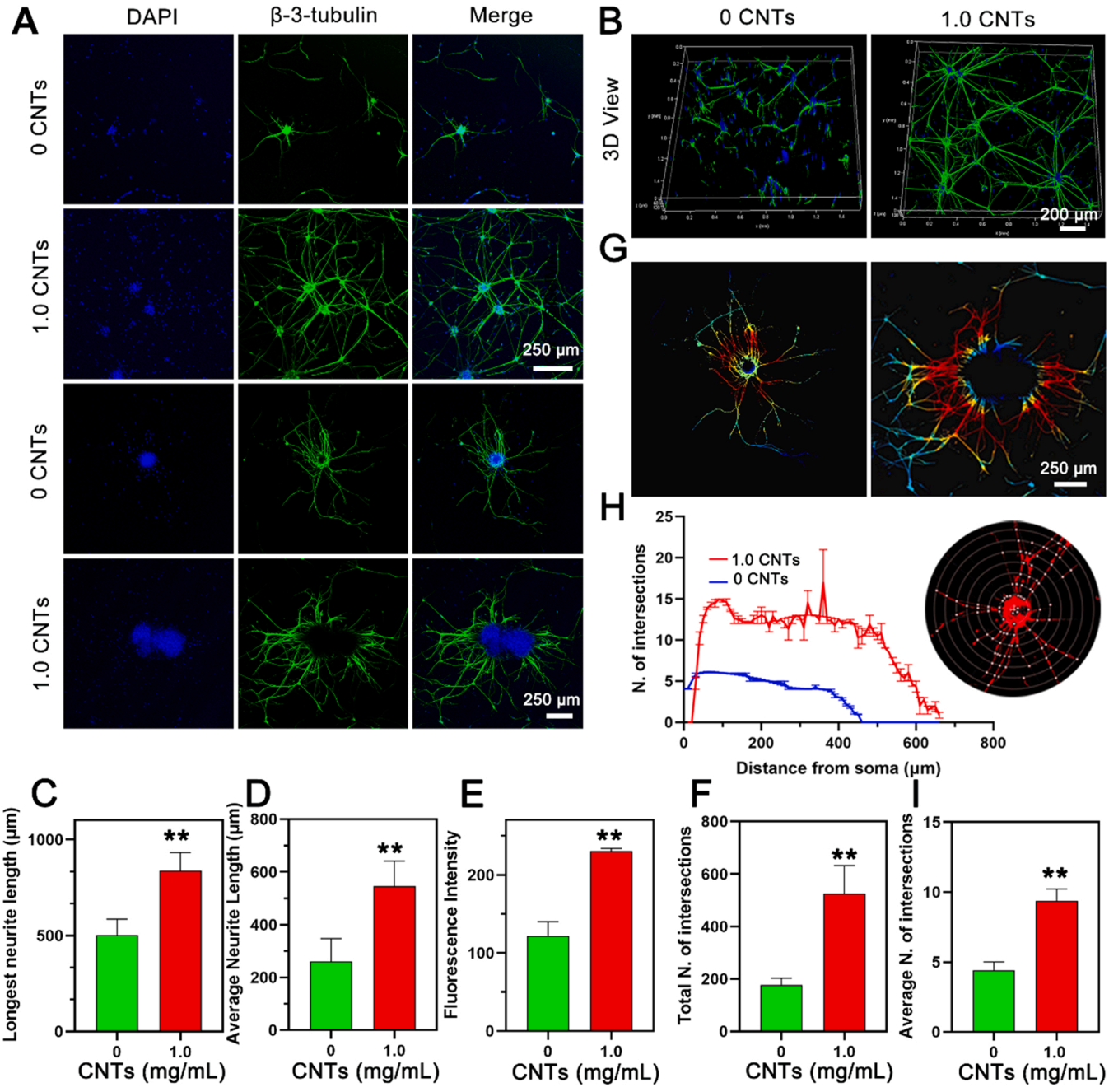

Fig. 4. Neurite development of DRG neurons on different scaffolds *in vitro*. (A) Representative fluorescence images cultured for 7 days. (B) 3D view. (C, D) Quantitative analysis of maximum and average neurite lengths. (E) Fluorescence intensity. (G) Sholl intersection mask based on Fig. 4A. (H) Sholl analysis plots of neuronal arborization. (F, I) Sholl analysis complexity of total and average DRG dendrites. All statistical data are represented as mean ± SD ($n = 3$; **$P < 0.01$ for comparison with 0 CNTs-group).

many central or peripheral nerve researches such as neuron-glia interaction and neurite outgrowth *in vitro* [36]. Therefore, DRG and DRG explants were isolated and cultured herein to assess whether the CNTs@GelMA/PLLA scaffold could promote the neurite outgrowth and dendritic development. Based on the results above, 1.0 mg/mL CNTs was selected as the optimal concentration for the following experiments. As shown in Fig. 4A, the DRGs and DRG explants in the 0 CNTs- and 1.0 CNTs-groups were immunostained with neuronal specific marker of β-3-tubulin after 7 days under ultrasonic vibration. The maximum neurite length in the 1.0 CNTs-group was 839.03 ± 92.94 μm, significantly longer than that in the 0 CNTs-group (502.91 ± 82.59 μm, $^{**}P < 0.01$, Fig. 4C). Additionally, average length of neurites in the 1.0 CNTs-group was 545.66 ± 95.71 μm, which was about twice longer than value of the 0 CNTs-group (261.34 ± 86.08 μm, $^{**}P < 0.01$, Fig. 4D). Furthermore, intensity of β-3-tubulin-positive neurons in the 1.0 CNTs-group was significantly higher than that of the 0 CNTs-group ($^{**}P < 0.01$, Fig. 4E). The results indicated that existence of CNTs within the scaffold was more effective in accelerating outgrowth of the neurites as compared with the pure polymer matrix.

To investigate promotion effect of the scaffold on complexity of neuron dendritic, semiautomatic Sholl analysis was implemented and 3D view of the DRGs cultured in each group was observed by confocal microscope. As shown in Fig. 4B, some neurites were sprouted out from cell body in 0 CNTs-group, but the spreading state was still slower and shorter than that appeared in the 1.0-CNTs group. Interestingly, the neurites grown in the CNTs@GelMA/PLLA scaffold were connected with each other and developed into neuronal networks after 7 days under ultrasonic vibration. Complexity of the DRG dendrites in each group was assessed by Sholl analysis (Fig. 4G, H**)**. Number of intersections in the 1.0 CNTs-group was higher than that in the 0 CNTs-group, meanwhile average and total numbers of intersections also showed a significantly increased number of neuronal processes in the 1.0 CNTs-group **(**Fig. 4F, I**)**. These results suggested that the CNTs@GelMA/PLLA scaffold has a positive effect on improving number and outgrowth of neurites, which might be ascribed to an enhanced connectivity of neurons after introduction of CNTs.

3.4. *In vivo peripheral nerve regeneration of CNTs@GelMA/PLLA scaffold*

To verify promotion effect of the CNTs@GelMA/PLLA scaffold on peripheral nerve regeneration, the scaffold was applied in a 10-mm rat sciatic nerve defect (Fig. S1). Electrophysiological analysis was applied to assess nerve conduction and motor function recovery (Fig. 5A), and the representative CMAP curves in the four groups were presented in Fig. 5C. Statistical analysis showed that the CMAP latency period in the CNTs@GelMA/PLLA and autograft groups was shorter than that in the control and GelMA/PLLA groups (Fig. 5D). In addition, peak value of the CMAP in the CNTs@GelMA/PLLA and autograft groups was much higher than the control and GelMA/PLLA groups (Fig. 5E). These results demonstrated that CMAP amplitude in the CNTs@GelMA/PLLA group was mostly close to the autograft circumstance, and such enhanced CMAP amplitude was correlated with the number of regenerated motor fibers and reinnervation in target muscles [37].

Moreover, function recovery of peripheral nerve defects *in vivo* was evaluated by walking track analysis and the SFI was calculated by the footprint parameters. Normally, SFI value reflects the degree of sciatic nerve dysfunction, which varies from − 100 to 0, where 0 represents normal function and − 100 represents complete function loss [26]. At shown in Figs. S2 and 5B, the SFI values in the CNTs@GelMA/PLLA and autograft groups at 6 weeks were − 56.10 ± 4.07 and − 55.99 ± 3.82, respectively, being significantly higher than those in the control (− 79.99 ± 3.99, $^{**}P < 0.01$) and GelMA/PLLA groups (− 71.41 ± 4.06, $^{**}P < 0.01$). At 12 weeks, the SFI values in the CNTs@GelMA/PLLA and autograft groups increased to − 39.57 ± 3.77 and − 35.54 ± 8.56, which were still higher than those in the control (−68.11 ± 3.68, $^{**}P < 0.01$) and GelMA/PLLA groups (−54.21 ± 5.48, $^{**}P < 0.01$, Fig. 5F, G). Therefore, compared with the blank control and GelMA/PLLA groups, better functional recovery and comparable repair level with the autograft situations was observed in the CNTs@GelMA/PLLA group.

To further explore impact of the CNTs@GelMA/PLLA scaffold on regeneration of nerve fibers and myelination, immunohistochemical staining was implemented on longitudinal and transverse sections of the repaired nerves. NF160 is a specific marker for nerve fibers, and MBP and S-100 are important indicators for myelinated Schwann cells. As shown in Fig. 6A, the regenerated nerve fibers (NF160-positive) and SCs (MBP-positive) were evenly distributed in the CNTs@GelMA/PLLA and autograft groups after 12 weeks. The transverse sections at the middle site were also immunostained and presented in Fig. 6B. Intensities of NF160 IF and S-100 IF in the CNTs@GelMA/PLLA and autograft groups were significantly higher than those in the control and GelMA/PLLA groups (Fig. 6C, D).

Detailed structures of the regenerated nerves in each group were observed from TEM images shown in Fig. 7A. Similar to the autograft group, axons and myelin sheaths of regenerated nerves in the CNTs@GelMA/PLLA group were homogeneously distributed. Myelin sheath thicknesses in the control and GelMA/PLLA groups were 277.81 ± 17.62 nm and 365.88 ± 27.63 nm, separately, much thinner than those of the CNTs@GelMA/PLLA (539.08 ± 52.21 nm) and autograft (609.17 ± 116.72 nm) groups (Fig. 7D). Furthermore, axon diameters in the CNTs@GelMA/PLLA and autograft groups were significantly larger than those in the control and GelMA/PLLA groups (Fig. 7E). Above-mentioned results fully demonstrated that nerve fibers were regenerated well and arranged orderly in the CNTs@GelMA/PLLA and autograft groups, while being sparse and disorganized in the other groups instead. Therefore, our proposed CNTs@GelMA/PLLA scaffold showed great potential as a platform for promoting peripheral nerve regeneration.

Usually, neuro-regulation plays an important role in keeping viability of the gastrocnemius muscle. Atrophy of the gastrocnemius muscle (GM) was also evaluated and Masson trichrome was conducted in the muscle fibers of cross-section areas in each group (Fig. 7B, C). Masson's trichrome results of gastrocnemius muscle in the current study showed larger muscle fibers in the CNTs@GelMA/PLLA and autograft groups as compared with the other groups. Weight percentages of GM in the CNTs@GelMA/PLLA and autograft groups were 62.77% ± 2.61% and 67.55% ± 3.75%, separately, which were much higher than those in the control (29.92% ± 4.36%) and GelMA/PLLA groups (43.32% ± 5.22%, $^{**}P < 0.01$, Fig. 7F). Similarly, percentages of muscle fiber areas were 78.12% ± 4.31% and 70.26% ± 4.32% in the autograft and CNTs@GelMA/PLLA groups, also being significantly higher than those in the control (51.06% ± 3.32%) and GelMA/PLLA groups (58.13% ± 3.37%, $^{**}P < 0.01$, Fig. 7G). As we know, the neural electrophysiological signals could not transmit through defect site in the control and GelMA/PLLA groups because of absenting electroconductive biomaterials. Thus, we speculated that the application of electroconductive CNTs helped to transmit electrical signals to target muscle, which partly avoided atrophy of the target muscle.

Bioelectricity is an indispensable part in cell or tissue metabolism. Recently, electroactive biomaterials including piezoelectric and conductive materials are regarded as a new generation of smart biomaterials because of their excellent performance on promoting tissue regeneration [25]. In the current study, the soft, self-powered and electroconductive scaffold was fabricated and proved positive effect on peripheral nerve repair. Next, the role of the scaffold on the repair of spinal cord injury will be further explored. Furthermore, many tissues such as bone, cartilage and skin show piezoelectrical property and the electroactive CNTs@GelMA/PLLA composite scaffold has a promising possibility of being applied in these tissues [38].

In our research, we found that the piezoelectric and conductive scaffold promoted the spread of SCs and the outgrowth of axons. The bipolar SCs were easily migratory and wrapped outside the nerve fibers

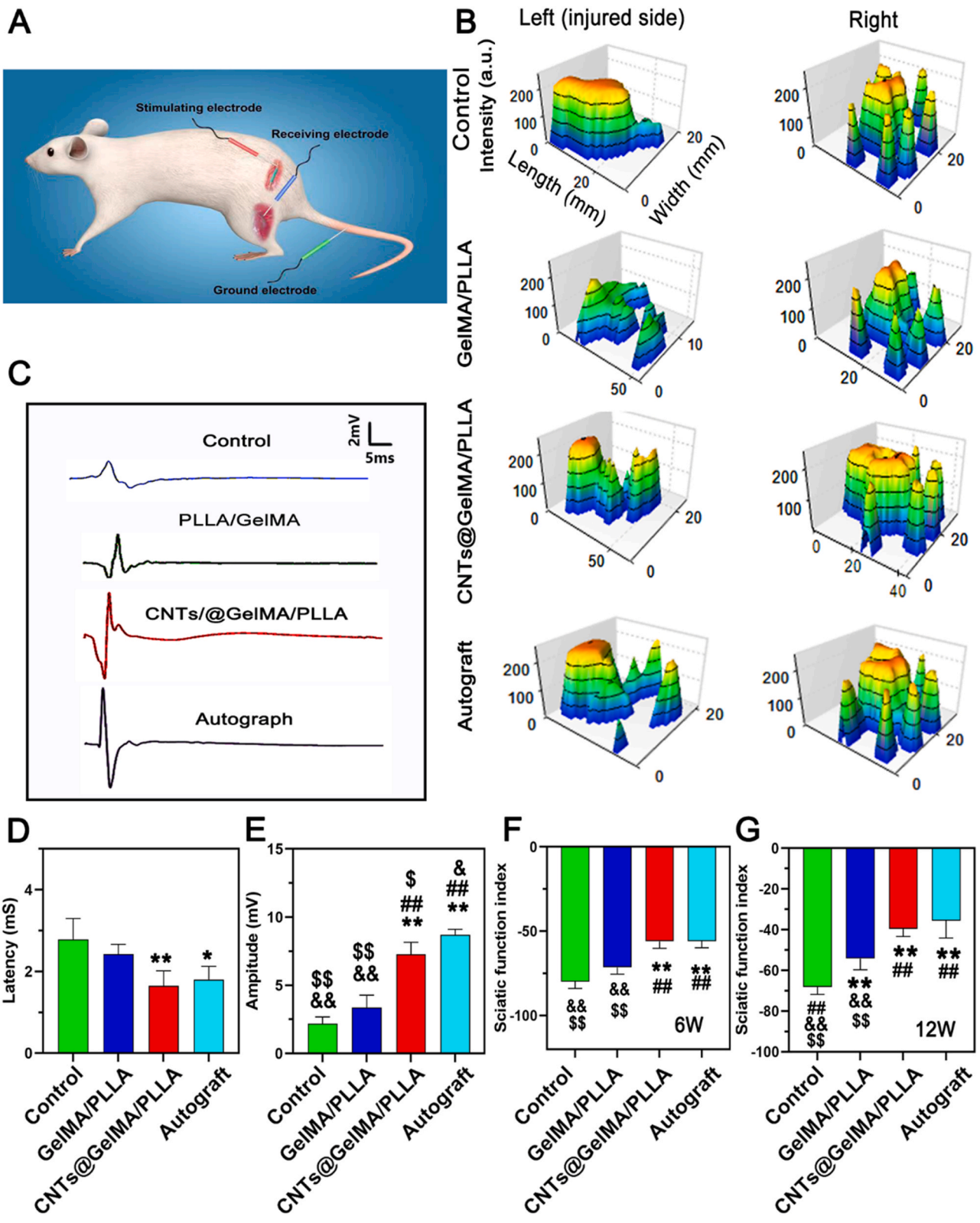

Fig. 5. Functional recovery of transected sciatic nerves. (A) Schematic illustration of electrophysiological examination on rats. (B) Footprint images of control, GelMA/PLLA, CNTs@GelMA/PLLA, and autograft groups at 12 weeks. (C–E) Latency and amplitude of CMAP in control, GelMA/PLLA, CNTs@GelMA/PLLA, and autograft groups at 12 weeks post-operation. (F–G) SFI values in different groups at 6 weeks and 12 weeks. (E) Evoked CMAP at 12 weeks post-operation. All statistical data are represented as mean ± SD ($n = 3$; $^{*}P < 0.05$ for comparison with the control group. $^{**}P < 0.01$ for comparison with the control group. $^{\#\#}P < 0.01$ for comparison with GelMA/PLLA group. $^{\&}P < 0.05$ for comparison with the CNTs@GelMA/PLLA group. $^{\&\&}P < 0.01$ for comparison with the CNTs@GelMA/PLLA group. $^{\$}P < 0.05$ for comparison with autograft group. $^{\$\$}P < 0.01$ for comparison with autograft group).

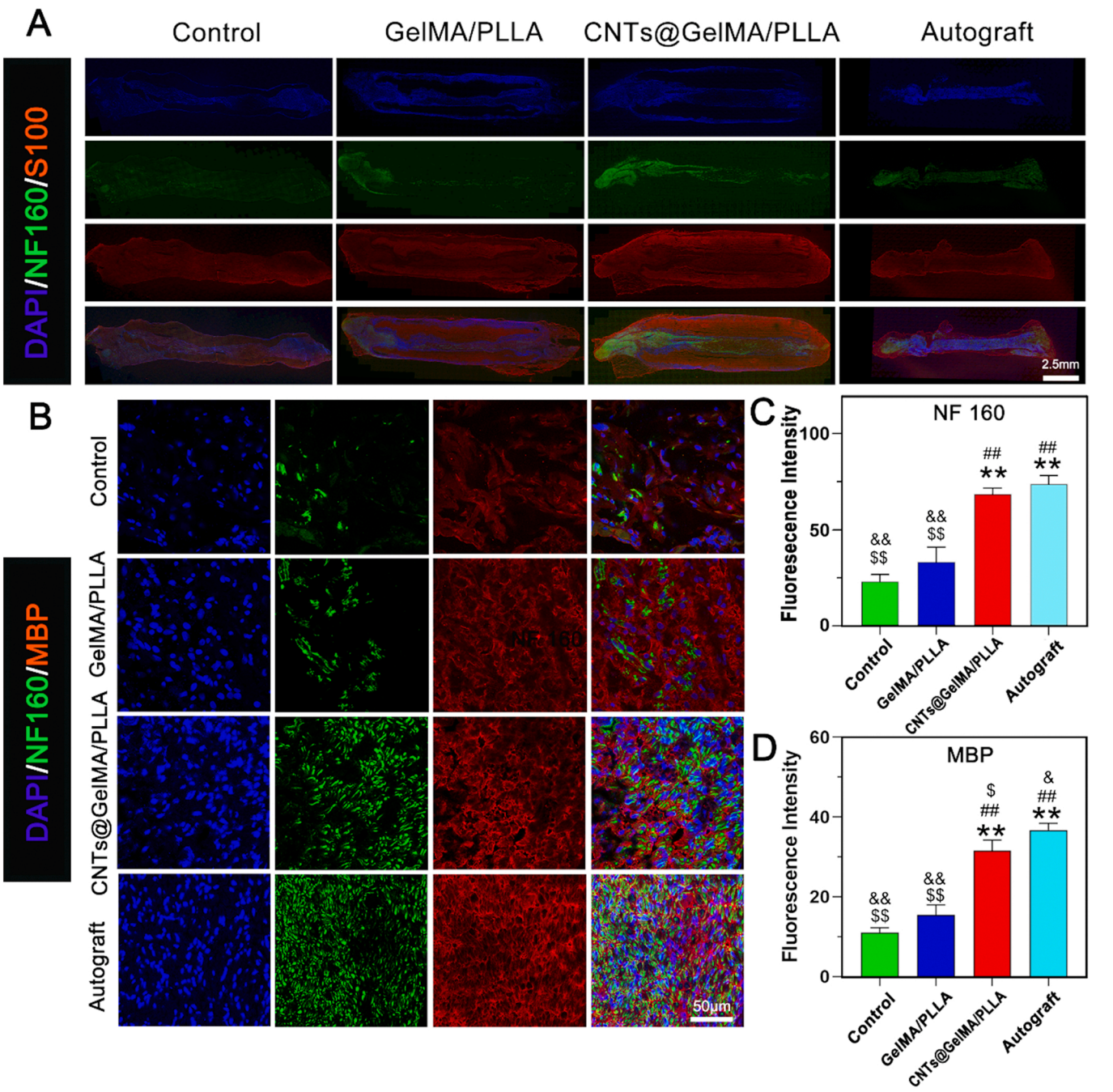

Fig. 6. Histological changes in injured sciatic nerve at three months after repair. (A) Immunofluorescence images of nerve fibers and SCs. (B) Immunostaining images of myelination at middle site. (C–D) Fluorescence intensity of NF160 and MBP. All statistical data are represented as mean ± SD ($n = 3$; $^{**}P < 0.01$ for comparison with the control group. $^{\#\#}P < 0.01$ for comparison with GelMA/PLLA group. $^{\&}P < 0.05$ for comparison with the CNTs@GelMA/PLLA group. $^{\&\&}P < 0.01$ for comparison with the CNTs@GelMA/PLLA group. $^{\$}P < 0.05$ for comparison with the autograft group. $^{\$\$}P < 0.01$ for comparison with the autograft group).

to induce myelin formation [39]. In addition, the number and length of nerve fibers were significantly enhanced in the piezoelectric and conductive scaffold. Therefore, the possible mechanism of piezoelectric and conductive signals promoting the repair of PNI could be explained by activating the remyelination of SCs and the outgrowth of nerve fibers. Additionally, the underlying molecular mechanism of piezoelectric and conductive signals has also been preliminarily explored. For example, growth factor receptor-bound protein-2 (GRB2) was an electrically-sensitive protein, and it was found that piezoelectric stimulation enhanced nerve regeneration by activating GRB2/RAS/MAPK pathway [40]. Moreover, electroconductive hydrogels were also demonstrated with ability of accelerating axon regeneration and remyelination by activating MEK/ERK signaling pathways [26]. In fact, the mechanism by which the piezoelectric and conductive signals promote nerve regeneration is still not fully understood [23,41]. More details about the underlying molecular mechanism of how the electroconductive scaffolds influenced nerve regeneration are required to be explored in the future.

4. Conclusions

In summary, a double-layer, self-powered, and electroconductive CNTs@GelMA/PLLA composite scaffold was successfully developed in the current study. As the CNTs concentration was chosen as 1.0 mg/mL,

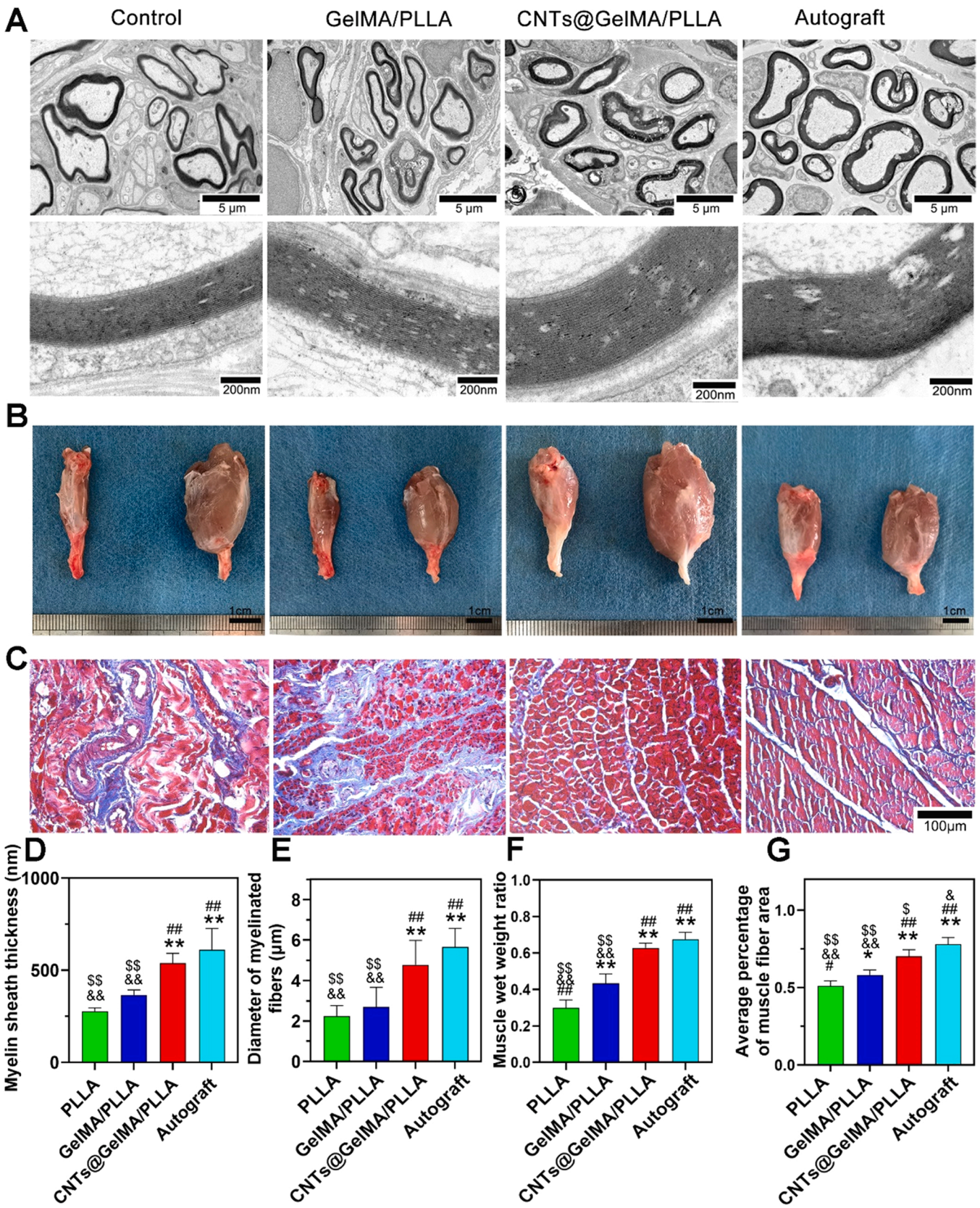

Fig. 7. Regeneration ability of sciatic nerve and GM. (A) TEM images of regenerated nerves in four groups. (B) Shape of GM in four groups (Left: untreated muscle tissue; Right: postoperative muscle tissue). (C) Masson trichrome staining of GM. (D) Wet weight percentage of GM in control, GelMA/PLLA, CNTs@GelMA/PLLA, and autograft groups. (D) Myelin sheath thicknesses, (E) axon diameter, (F) weight percentages, and (G) percentages of muscle fiber areas in four groups. All statistical data are represented as mean ± SD ($n = 3$; * $P < 0.05$ for comparison with control group. ** $P < 0.01$ for comparison with control group. $^{\#}P < 0.05$ for comparison with GelMA/PLLA group. $^{\#\#}P < 0.01$ for comparison with GelMA/PLLA group. $^{\&}P < 0.05$ for comparison with CNTs@GelMA/PLLA group. $^{\&\&}P < 0.01$ for comparison with CNTs@GelMA/PLLA group. $^{\$}P < 0.05$ for comparison with autograft group. $^{\$\$}P < 0.01$ for comparison with autograft group).

the scaffold exhibited an appropriate stiffness, sensitive piezoelectricity, excellent conductivity, and ideal biocompatibility. *In vitro* study suggested that such biomimetic scaffold significantly promoted growth and myelination of SCs as well as neurite growth of DRGs. Besides, application of the scaffold significantly facilitated peripheral nerve regeneration and functional recovery *in vivo*. Taken together, the well-designed composite scaffold may serve as an alternative of autologous nerve in the repair of peripheral nerve defect.

CRediT authorship contribution statement

Yafeng Yang: Conceptualization, Methodology, Formal analysis, Investigation, Writing – original draft, Writing – review & editing. **Xin Yin:** Methodology, Formal analysis, Writing – original draft, Writing – review & editing. **Huadong Wang:** Conceptualization, Investigation, Writing – original draft, Writing – review & editing. **Wenqi Qiu:** Methodology, Writing – original draft, Writing – review & editing. **Li Li:** Investigation, Writing – original draft, Writing – review & editing. **Fenglu Li:** Methodology, Writing – original draft, Writing – review & editing. **Yizhu Shan:** Conceptualization, Writing – original draft, Writing – review & editing. **Ziteng Zhao:** Methodology, Formal analysis. **Guoliang Shi:** Methodology, Formal analysis. **Zhou Li:** Conceptualization, Writing – original draft, Writing – review & editing. **Jidong Guo:** Conceptualization, Investigation, Supervision, Funding acquisition. **Jin Zhang:** Conceptualization, Formal analysis, Investigation, Writing – original draft, Writing – review & editing. **Yantao Zhao:** Conceptualization, Methodology, Formal analysis, Supervision, Funding acquisition, Writing – original draft, Writing – review & editing.

Declaration of Competing Interest

The authors declare that they have no known competing financial interests or personal relationships that could have appeared to influence the work reported in this paper.

Data Availability

No data was used for the research described in the article.

Acknowledgements

This work was financially supported by the National Key R&D Program of China (Grant no. 2022YFB3808000/2022YFB3808001), the National Natural Science Foundation of China (Grant nos. 82071356, 51903050, 82151312 and 21874024), the Military Young Scholar Medical Research Foundation of China (No. 20QNPY104), and the Beijing Municipal Natural Science Foundation (No. 7224345). The authors also gratefully acknowledged the kindly financial support provided by the Top Young Talents of Foal Eagle Program of Fujian Province and the Youth Promotion Talent Project of Fujian Province to Jin Zhang.

Appendix A. Supporting information

Supplementary data associated with this article can be found in the online version at doi:10.1016/j.nanoen.2022.108145.

References

[1] L. Luo, Y. He, L. Jin, Y. Zhang, F.P. Guastaldi, A.A. Albashari, F. Hu, X. Wang, L. Wang, J. Xiao, Bioact. Mater. 6 (2021) 638–654, https://doi.org/10.1016/j.bioactmat.2020.08.028.
[2] M. Yu, G. Gu, M. Cong, M. Du, W. Wang, M. Shen, Q. Zhang, H. Shi, X. Gu, F. Ding, Acta Biomater. 134 (2021) 190–203, https://doi.org/10.1016/j.actbio.2021.07.026.
[3] F. Jin, T. Li, T. Yuan, L. Du, C. Lai, Q. Wu, Y. Zhao, F. Sun, L. Gu, T. Wang, Adv. Mater. 33 (2021) 2104175, https://doi.org/10.1002/adma.202104175.
[4] F. Han, X. Ma, Y. Zhai, L. Cui, L. Yang, Z. Zhu, Y. Hao, G. Cheng, Adv. Healthc. Mater. 10 (2021) 2100027, https://doi.org/10.1002/adhm.202100027.
[5] S. Grossemy, P.P. Chan, P.M. Doran, Adv. Biol. 5 (2021) 2000136, https://doi.org/10.1002/adbi.202000136.
[6] Z. Guo, C. Sun, H. Yang, H. Gao, N. Liang, J. Wang, S. Hu, N. Ren, J. Pang, J. Wang, Adv. Sci. 9 (2022) 2104424, https://doi.org/10.1002/advs.202104424.
[7] L. He, Z. Sun, J. Li, R. Zhu, B. Niu, K.L. Tam, Q. Xiao, J. Li, W. Wang, C.Y. Tsui, Biomaterials 268 (2021), 120585, https://doi.org/10.1016/j.biomaterials.2020.120585.
[8] J. Zhang, X. Zhang, C. Wang, F. Li, Z. Qiao, L. Zeng, Z. Wang, H. Liu, J. Ding, H. Yang, Adv. Healthc. Mater. 10 (2021) 2000604, https://doi.org/10.1002/adhm.202002255.
[9] A. Singh, A. Raghav, P.A. Shiekh, A. Kumar, Bioact. Mater. 6 (2021) 2231–2249, https://doi.org/10.1016/j.bioactmat.2021.01.008.
[10] Y. Sun, Q. Quan, H.Y. Meng, Y.D. Zheng, J. Peng, Y.X. Hu, Z.X. Feng, X. Sang, K. Qiao, W. He, X.Q. Chi, L. Zhao, Adv. Healthc. Mater. 8 (2019), https://doi.org/10.1002/adhm.201900127.
[11] R.Q. Yuan, N. Yang, S.W. Fan, Y.R. Huang, D. You, J.R. Wang, Q.L. Zhang, C. L. Chu, Z.Z. Chen, L. Liu, L.Q. Ge, Small 17 (2021), https://doi.org/10.1002/smll.202103997.
[12] M.T. Chorsi, E.J. Curry, H.T. Chorsi, R. Das, J. Baroody, P.K. Purohit, H. Ilies, T. D. Nguyen, Adv. Mater. 31 (2019) 1802084, https://doi.org/10.1002/adma.201802084.
[13] Z. Liu, X. Wan, Z.L. Wang, L. Li, Adv. Mater. 33 (2021) 2007429, https://doi.org/10.1002/adma.202007429.
[14] Y. Liu, G. Dzidotor, T.T. Le, T. Vinikoor, K. Morgan, E.J. Curry, R. Das, A. McClinton, E. Eisenberg, L.N. Apuzzo, Sci. Transl. Med. 14 (2022) eabi7282, https://doi.org/10.1126/scitranslmed.abi7282.
[15] W. Liu, X. Li, Y. Jiao, C. Wu, S. Guo, X. Xiao, X. Wei, J. Wu, P. Gao, N. Wang, Y. Lu, Z. Tang, Q. Zhao, J. Zhang, Y. Tang, L. Shi, Z. Guo, ACS Appl. Mater. Interfaces 12 (2020) 51885–51903, https://doi.org/10.1021/acsami.0c10957.
[16] Y.-H. Lai, Y.-H. Chen, A. Pal, S.-H. Chou, S.-J. Chang, E.-W. Huang, Z.-H. Lin, S.-Y. Chen, Nano Energy 90 (2021), 106545, https://doi.org/10.1016/j.nanoen.2021.106545.
[17] X. Lu, C. Sun, L. Chen, Z. Feng, H. Gao, S. Hu, M. Dong, J. Wang, W. Zhou, N. Ren, Small 18 (2022) 2107236, https://doi.org/10.1002/smll.202107236.
[18] S.P. Lacour, G. Courtine, J. Guck, Nat. Rev. Mater. 1 (2016) 1–14, https://doi.org/10.1038/natrevmats.2016.63.
[19] E. Axpe, G. Orive, K. Franze, E.A. Appel, Nat. Commun. 11 (2020) 1–4, https://doi.org/10.1038/s41467-020-17245-x.
[20] C.M. Madl, B.L. LeSavage, R.E. Dewi, C.B. Dinh, R.S. Stowers, M. Khariton, K. J. Lampe, D. Nguyen, O. Chaudhuri, A. Enejder, Nat. Mater. 16 (2017) 1233–1242, https://doi.org/10.1038/nmat5020.
[21] Y. Hu, W. Chen, H. Yin, X. Chen, J. Cai, J. Guo, S. Zhou, R. Chai, M. Tang, Mater. Today Nano 18 (2022), 100181, https://doi.org/10.1016/j.mtnano.2022.100181.
[22] Y. Zheng, G. Wu, L. Chen, Y. Zhang, Y. Luo, Y. Zheng, F. Hu, T. Forouzanfar, H. Lin, B. Liu, Bioact. Mater. 6 (2021) 627–637, https://doi.org/10.1016/j.bioactmat.2020.08.026.
[23] L. Ye, H. Ji, J. Liu, C.H. Tu, M. Kappl, K. Koynov, J. Vogt, H.J. Butt, Adv. Mater. 33 (2021) 2102981, https://doi.org/10.1002/adma.202102981.
[24] B.S. Spearman, V.H. Desai, S. Mobini, M.D. McDermott, J.B. Graham, K.J. Otto, J. W. Judy, C.E. Schmidt, Adv. Funct. Mater. 28 (2018) 1701713, https://doi.org/10.1002/adfm.201701713.
[25] Z. Liu, X. Wan, Z.L. Wang, L. Li, Adv. Mater. 33 (2021), e2007429, https://doi.org/10.1002/adma.202007429.
[26] C. Liu, L. Fan, Z.M. Tian, H.Q. Wen, L. Zhou, P.F. Guan, Y. Luo, C.C. Chan, G.X. Tan, C.Y. Ning, L.M. Rong, B. Liu, vol. 6, 2021, pp. 3892–903. ⟨https://doi.org/10.1016/j.bioactmat.2021.03.034⟩.
[27] J.D. Shi, Y. Fang, Adv. Mater. 31 (2019), https://doi.org/10.1002/adma.201804895.
[28] J.H. Koo, J.K. Song, D.H. Kim, D. Son, ACS Mater. Lett. 3 (2021) 1528–1540, https://doi.org/10.1021/acsmaterialslett.1c00438.
[29] S.M. Deupree, M.H. Schoenfisch, Acta Biomater. 5 (2009) 1405–1415, https://doi.org/10.1016/j.actbio.2009.01.025.
[30] X.-L. Cai, C.-H. Liu, J. Liu, Y. Lu, Y.-N. Zhong, K.-Q. Nie, J.-L. Xu, X. Gao, X.-H. Sun, S.-D. Wang, Nanomicro Lett. 9 (2017), https://doi.org/10.1007/s40820-017-0149-1.
[31] J. Shi, W. Wang, Z. Feng, D. Zhang, Z. Zhou, Q. Li, Polymer 175 (2019) 152–160, https://doi.org/10.1016/j.polymer.2019.05.008.
[32] M.M. Maciel, S. Ribeiro, C. Ribeiro, A. Francesko, A. Maceiras, J.L. Vilas, S. Lanceros-Méndez, Compos. B Eng. 139 (2018) 146–154, https://doi.org/10.1016/j.compositesb.2017.11.065.
[33] X. Liu, J. Wang, Z. Shen, H. Zhang, B. Li, Y. Zhang, X. Zhang, J. Alloy. Compd. 927 (2022), https://doi.org/10.1016/j.jallcom.2022.166832.
[34] T. Ma, Y. Yang, X. Quan, L. Lu, B. Xia, J. Gao, F. Qi, S. Li, L. Zhao, L. Mei, Y. Zheng, Y. Shen, Z. Luo, Y. Jin, J. Huang, Theranostics 10 (2020) 8957–8973, https://doi.org/10.7150/thno.45035.
[35] N. Tricaud, Front. Cell. Neurosci. 11 (2017) 414, https://doi.org/10.3389/fncel.2017.00414.
[36] M. Fornaro, H. Sharthiya, V. Tiwari, J. Vis. Exp. (2018), https://doi.org/10.3791/56757.
[37] J. Du, J. Liu, S. Yao, H. Mao, J. Peng, X. Sun, Z. Cao, Y. Yang, B. Xiao, Y. Wang, P. Tang, X. Wang, Acta Biomater. 55 (2017) 296–309, https://doi.org/10.1016/j.actbio.2017.04.010.
[38] D. Kim, S.A. Han, J.H. Kim, J.H. Lee, S.W. Kim, S.W. Lee, Adv. Mater. 32 (2020) 1906989, https://doi.org/10.1002/adma.201906989.

[39] S.E. Park, J. Ahn, H.-E. Jeong, I. Youn, D. Huh, S. Chung, NPG Asia Mater. 13 (2021) 2, https://doi.org/10.1038/s41427-020-00273-w.
[40] R. Mao, B. Yu, J. Cui, Z. Wang, X. Huang, H. Yu, K. Lin, S.G.F. Shen, Nano Energy 98 (2022), 107322, https://doi.org/10.1016/j.nanoen.2022.107322.
[41] Y. Luo, L. Fan, C. Liu, H. Wen, S. Wang, P. Guan, D. Chen, C. Ning, L. Zhou, G. Tan, Bioact. Mater. 7 (2022) 98–111, https://doi.org/10.1016/j.bioactmat.2021.05.039.